Anisotropic Biaxial Creep of Textured Nb-Modified Zircaloy-4 Tubing

Nilesh Kumar, Kaitlin Grundy, Boopathy Kombaiah, Baifeng Luan and Korukonda Murty

Abstract Biaxial creep of Nb-modified Zircaloy-4 (HANA-4) tubing is investigated at varied ratios of hoop and axial stresses at a constant temperature of 500 °C using internal pressurization superimposed with axial load while monitoring the hoop and axial strains using non-contact laser telemetric extensometer and linear variable differential transducer, respectively. Steady-state creep rates along the hoop and axial directions were evaluated in the power-law creep regime from which the creep locus was derived at a constant energy of dissipation. The resulting creep locus was compared with that predicted by the anisotropy parameters, R and P in the Hill's formulation for generalized stress for anisotropic materials. Crystallographic texture of the tubing was characterized using electron backscatter diffraction technique. Research is supported by NSF grant #DMR0968825.

Keywords Biaxial creep · Zirconium alloy · Cladding material · Anisotropy

N. Kumar (✉) · K. Grundy · K. Murty
Department of Nuclear Engineering, NC State University, Raleigh, NC, USA
e-mail: nkumar7@ncsu.edu

K. Grundy
e-mail: kgrundy00@gmail.com

B. Kombaiah
Carnegie Mellon University, Pittsburgh, USA
e-mail: bkombaiah@gmail.com

B. Luan
School of Materials Science and Engineering, Chongqing University, Chongqing 400030, China
e-mail: bfluan@cqu.edu.cn

K. Grundy
BWX Technologies, Lynchburg, VA, USA

I. Charit et al. (eds.), *Mechanical and Creep Behavior of Advanced Materials*,
The Minerals, Metals & Materials Series, DOI 10.1007/978-3-319-51097-2_2

Introduction

Due to looming threat of global warming on earth's ecosystem, nuclear energy is receiving ever-increasing attention worldwide. In a recently concluded Paris COP21 climate summit to discuss global warming, Nuclear for Climate delegation underscored the role nuclear energy would play in mitigating the menace of global warming [1, 2]. However, before nuclear industry becomes mainstream energy source globally, it has to overcome several barriers in the path of its growth. The materials in and around nuclear reactor core work under extreme environmental conditions. Due to the presence of gamma ray radiations, neutron, and other fission products, high stresses (thermal and mechanical), high temperature, and corrosive atmosphere (due to coolants), structural materials operate under very harsh conditions. The ongoing effort for prolonging the life of existing nuclear reactors, higher fuel burnups, and demand for advanced reactors with superior performance and safety has culminated in a greater push for, among many things, developing advanced materials to cater the need of existing and next generation nuclear reactors [3]. The aging and degradation associated with materials are the main limiting factors for continued and sustained safe operation of nuclear reactors currently in use. Any new material developed for current and future fleet of nuclear reactors must have enough resistance to major materials degradation phenomena such as thermal creep, cyclic fatigue, creep-fatigue, radiation damage, and corrosion. In order to develop advanced materials for structural applications, thus, it becomes imperative to understand the fundamentals of aging and degradation mechanisms and factors controlling such mechanisms. The improved understanding of aging and degradation mechanisms will allow design of materials capable of resisting the degradation phenomena mentioned earlier.

Nuclear fuel cladding is a critical component of a nuclear reactor core. Nuclear industry has primarily relied on zirconium (Zr) based alloys for manufacturing cladding tubes [4, 5]. While Zircaloys have been an effective cladding material in light water reactors (LWRs), in recent past, in the face of demand for better and safer nuclear reactors, this has led to the development of cladding materials that can more efficiently face these conditions [6, 7]. Specifically, an increase in the corrosion resistance than that achieved by Zircaloys is desirable due to the fact that waterside corrosion is a major limitation on higher fuel burn-up [6]. While the corrosion resistance shown by Zircaloys meets the current nuclear reactors' criteria, there must be an improvement if an extension in fuel burn-up and nuclear reactor life are desired [8]. The Korea Atomic Energy Research Institute (KAERI) along with Korea Nuclear Fuel Company (KNFC) has carried out extensive research to determine alloying elements and compositions, which optimize the corrosion resistance of zirconium alloys [9]. This led to research in niobium-modified zirconium alloys due to the corresponding increase in corrosion resistance and strength [10]. Initially, zirconium alloys with the addition of niobium were predominantly used in Russian water reactors (RBMK and VVER). The success of the Zr-Nb alloys in maintaining long term corrosion resistance and mechanical

properties while preserving the nuclear properties for extended fuel cycles led to Canadian researchers to develop zirconium alloys with 2.5 wt% niobium to be used in their PHWR (CANDU) reactors [10]. Even more recently, there has been a further development in niobium modified zirconium alloys (Zirlo@ and M5) which are used in USA and European reactors [10].

Owing to hexagonal close packed crystal structure of zirconium alloys, they possess limited slip systems [11] resulting in preferred orientation or texture during fabrication process of the cladding tubes. Texture not only affects the formability of the material during fabrication process but also affects in-service performance. Properties such as the yield strength, creep, fatigue life, stress corrosion cracking resistance, hydride orientation, and irradiation induced growth behavior are strongly influenced by texture [12, 13]. The factors influencing texture can be broadly grouped into two categories—material and process variables. Crystal structure, solute content, second phase particles, and initial grain size are a few examples of material related variables [12–14]. The process variables are extent of deformation, stress and strain states. It suggests that a change in processing route and/or alloy will lead to introduction of a different texture in the material.

The present research focuses on thermal creep evaluation of an Nb-modified Zircaloy commonly referred to as HANA-4 (High Performance Alloy for Nuclear Applications, developed by KAERI). In the past, most of the studies related to biaxial creep are either on Zircaloy-4 or some other materials such as titanium or ferrous based alloys [15–22]. Being a new alloy, the microstructure and hence texture is expected to be different for this alloy. Due to absence of prior study on this alloy about the effect of texture on creep behavior, it becomes imperative to understand creep anisotropy of the alloy. Since fuel cladding tubes experience multiaxial loading in service, the creep deformation behavior of HANA-4 tubes has been evaluated under biaxial loading conditions.

Material and Experimental Procedure

HANA-4 alloy tube used in the present investigation was received from KAERI in cold-worked and stress-relieved condition. The chemical composition of the alloy is provided in Table 1 that also includes the chemistry of a Zircaloy-4 for comparison purpose. Before performing biaxial creep tests, these tubes were subjected to annealing heat-treatment at 537 °C for 4 h in argon atmosphere. The outer diameter and thickness of the wall of the tube were 9.50 and 0.57 mm, respectively.

Table 1 Comparison of HANA-4 and Zircaloy-4 composition [9]

Alloy	Composition in weight %				
	Nb	Sn	Fe	Cr	Zr
HANA-4	1.45	0.41	0.22	0.10	Bal.
Zircaloy-4	–	1.50	0.22	0.10	Bal.

A thin-wall approximation was applied to the HANA-4 tubing in the calculation of axial and hoop stresses because the wall thickness (t) to outer diameter (D_o) ratio was less than 0.1. It results in biaxial stress of the state as the radial stress can be assumed to be negligible due to the geometry of the tube. Biaxial stress state was imposed by applying axial load and closed-end internal pressurization of the HANA-4 tubes using argon gas. Biaxial creep tests were carried out at different stress ratios (α) defined as

$$\alpha = \frac{\sigma_\theta}{\sigma_z} \tag{1}$$

where σ_θ, and σ_z are hoop and axial stress, respectively. The following expressions were used to calculate σ_θ and σ_z and the stress ratio was varied from 0 to 2 during the biaxial creep tests,

$$\sigma_\theta = \frac{P(D_o^2 + D_i^2)}{D_o^2 - D_i^2} \tag{2}$$

and

$$\sigma_z = \frac{\sigma_\theta}{2} + \frac{W}{\pi\left(D_o^2 - D_i^2\right)} \tag{3}$$

where P is the applied internal pressure of the tubing, W applied axial load, D_o outer diameter, and D_i internal diameter of the tube [19].

The biaxial creep experiments were conducted on an ATS model-2330 lever arm (ratio 20:1) machine in combination with an internal pressurization system which floods the hollow tube with argon gas (Fig. 1). The pressure system utilized a gas booster and an air compressor capable of achieving up to 17,000 psi. Other than the argon gas inlet, the tubing was closed end by use of Swagelock fittings. The test samples were enclosed in a high temperature furnace to heat the samples to the desired temperature of 500 °C. Temperature readings were obtained through attaching two K-type thermocouples to the tube with an uncertainty of ±2 °C. The change in dimensions of the tube along axial and radial directions were measured using linear variable differential transducer (LVDT) and laser telemetric extensometer, Beta Lasermike model 162. The axial and hoop displacement data were continuously logged into a computer using a data acquisition system.

Microstructural examination of the HANA-4 alloy in annealed condition was carried out using electron backscatter diffraction (EBSD) and transmission electron microscopy (TEM: 200 keV JEOL 2010F). The TEM samples were prepared using twin-jet electropolishing technique at −60 °C and 25 V in an electrolytic solution consisting of 30 mL sulphuric acid, 1 mL hydrofluoric acid, and 470 mL methanol.

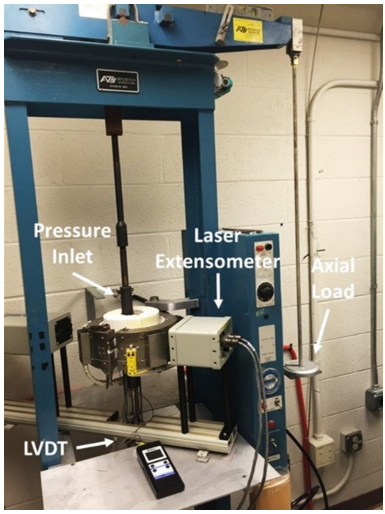

Fig. 1 Biaxial creep experimental set-up

Results and Discussion

Microstructure

The EBSD micrograph for the recrystallized HANA-4 alloy is shown in Fig. 2a. Thick black lines in the micrograph represent high angle grain boundaries. The color associated with each grain represents a crystallographic direction parallel to radial direction of the tube and it can be read from the inverse pole figure present as an inset in the lower left hand corner of Fig. 2a. The grain size distribution in terms of area fraction is included in Fig. 2b. The experimental distribution curve is curve fitted with a Gaussian distribution, and based on this distribution, the average grain size was found to be 3.6 ± 2.5 μm. The pole figures in Fig. 2c, d indicate that grains in the tube have preferred orientation. The basal pole figure shows that basal planes are tilted ∼35° from the radial direction towards the hoop direction of the tube (Fig. 2c). Although Fig. 2d shows prism planes are preferably oriented with maximum intensity being slightly away from the axial direction, the peak intensity of prism poles are very small compared to that of basal poles [23].

The TEM image included in Fig. 3a revealed round shaped precipitates distributed inter- and intra-granularly in the recrystallized alloy. About 500 precipitates were considered for precipitate size distribution (Fig. 3b) and a log-normal distribution was found to represent the precipitate size distribution the best. Average precipitate size was found to be 57 ± 34 nm. Boopathy and Murty have carried out a detailed analysis of these precipitates in this alloy and have found that the crystal structure of the precipitates were body-centered cubic and chemical composition (in at.%) was Nb-17Zr-0.2Cr-0.2Fe [23].

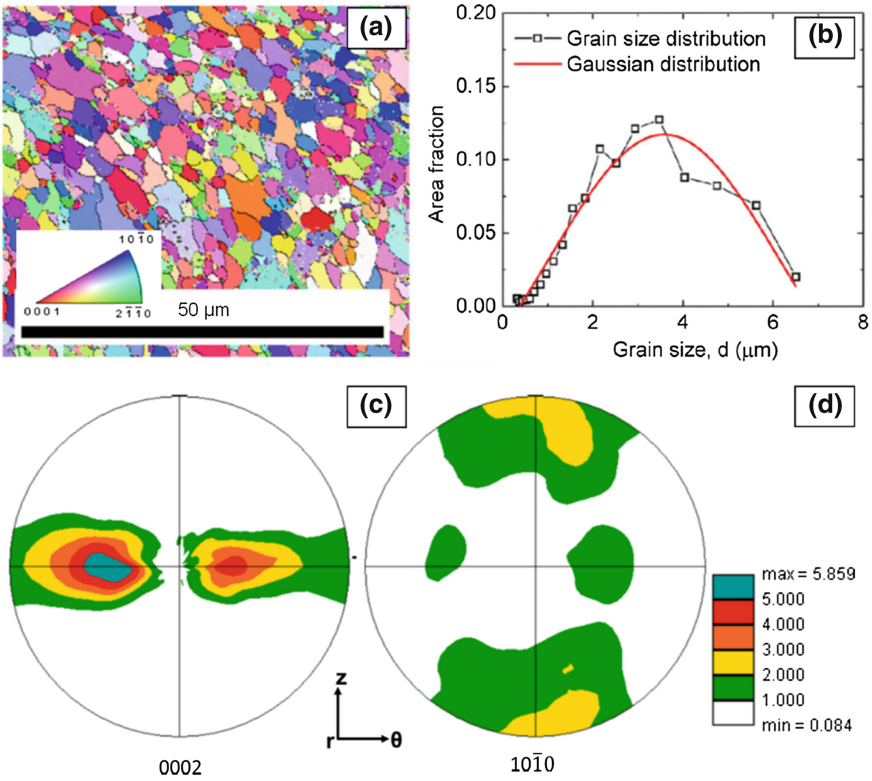

Fig. 2 **a** EBSD micrograph and **b** grain size (area fraction) distribution of HANA-4 alloy in recrystallized condition, **c** {0002} basal pole figure, and **d** {10-10} prismatic pole figure; r = radial direction, θ = tangential direction, z = axial direction

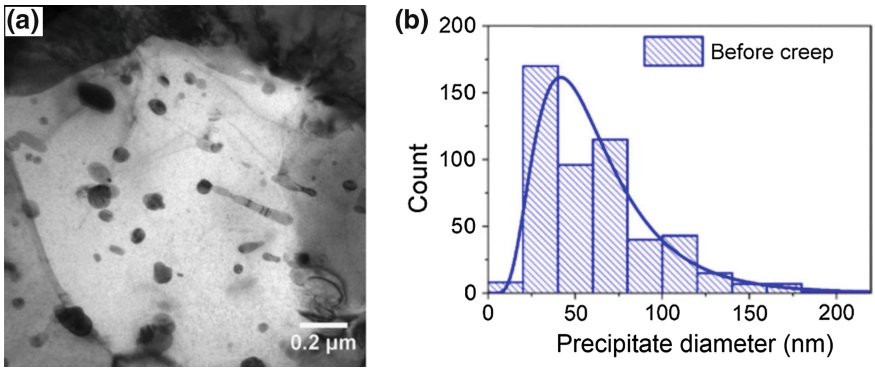

Fig. 3 **a** TEM micrograph showing shape, size, and spatial distribution of nanosized precipitates and **b** histogram showing precipitate size distribution in recrystallized HANA-4 alloy

Biaxial Creep Results

Figure 4 shows creep deformation characteristics of HANA-4 alloy. Figure 4a shows the variation of creep strain along axial direction whereas the change in hoop strain is included in Fig. 4b. As expected, with increase in stress (axial and hoop), the rate of creep deformation increased. The first derivatives of the curves which provides strain-rate have been plotted in Fig. 5.

Figure 6 shows creep curves as a function of stress ratio ($\alpha = \sigma_\theta/\sigma_z$). It shows that for stress ratios less than 1, the alloy deforms at faster rate along axial direction. At the stress ratio of 1, one can note that the creep curve corresponding to hoop direction lies above the curve corresponding to axial direction. However, for all practical purposes the rate of deformation along both directions can be assumed identical. It is indicative of planar isotropy. At the stress ratios above 1, one can

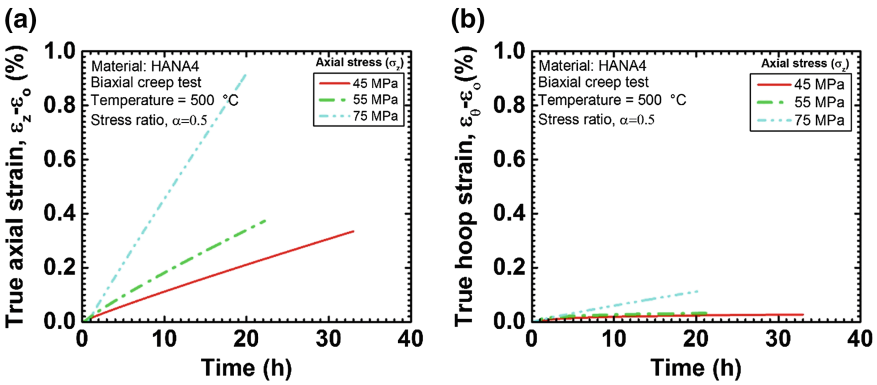

Fig. 4 Creep curves from biaxial creep tests of HANA-4 alloy at 500 °C and stress ratio, α = 0.5; creep curves **a** axial true strain and **b** hoop true strain

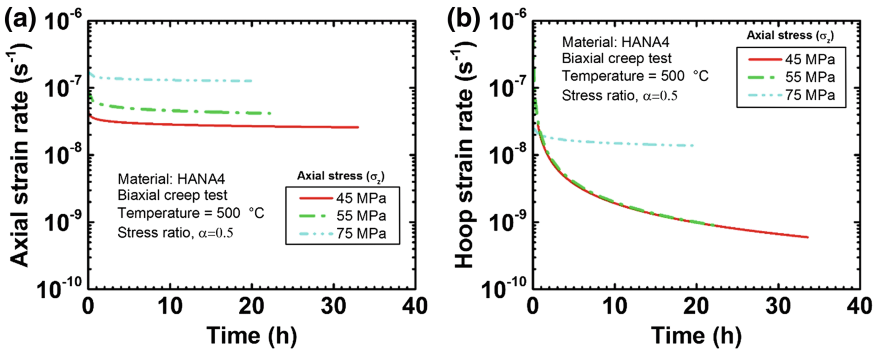

Fig. 5 Strain rate variation during biaxial creep tests of HANA-4 alloy at 500 °C and stress ratio, α = 0.5; **a** axial strain rate and **b** hoop strain rate

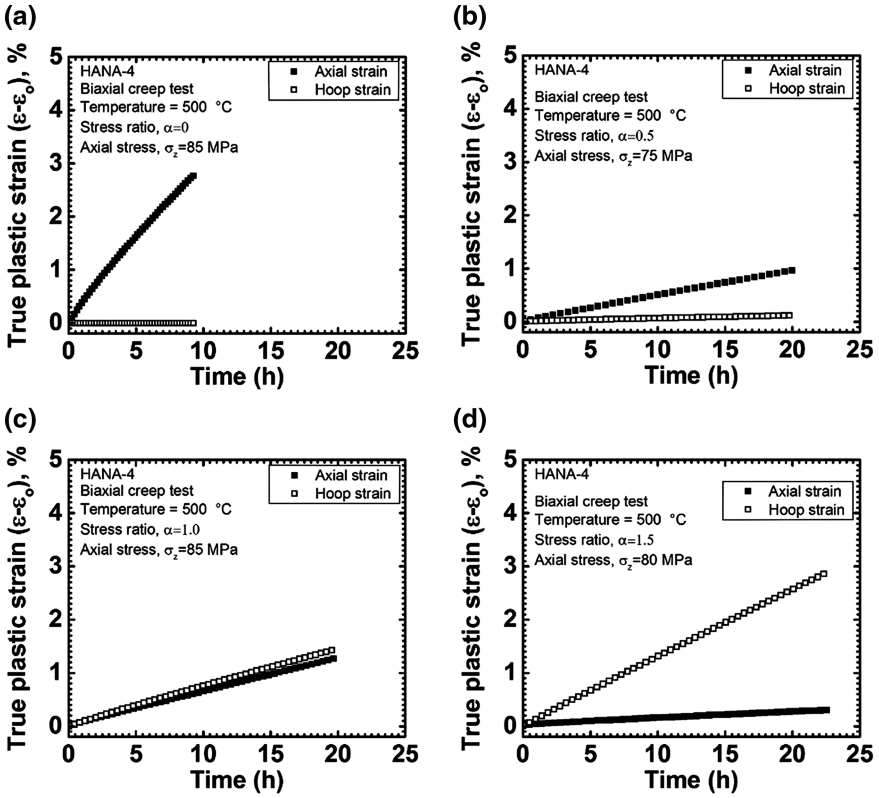

Fig. 6 Creep curves (plastic strain vs. time) as a function of stress ratio for HANA-4 alloy at 500 °C

note higher rate of deformation along hoop direction at any point of time during the creep deformation.

Evaluation of Creep Anisotropy Parameters

A number of theories have been put forth to deal with yielding of materials under complex stress states. A comprehensive treatment to the yield criterion for anisotropic material was first put forth by Hill in 1948 [24]. It is given as follows.

$$F(\sigma_y - \sigma_z)^2 + G(\sigma_z - \sigma_x)^2 + H(\sigma_x - \sigma_y)^2 + 2L\tau_{yz}^2 + 2M\tau_{zx}^2 + 2N\tau_{xy}^2 = 1 \qquad (4)$$

It is nothing but a generalized form of Von Mises yield criterion. Later on Eq. (4) was modified by Backofen and others as follows [17, 19].

$$\sigma_g = \frac{\mathrm{R}(\sigma_r - \sigma_\theta)^2 + \mathrm{RP}(\sigma_\theta - \sigma_z)^2 + \mathrm{P}(\sigma_z - \sigma_r)^2}{\mathrm{P}(\mathrm{R} + 1)} \tag{5}$$

where R and P are anisotropy parameters defined as

$$\mathrm{R} = \left(\frac{\varepsilon_\theta}{\varepsilon_r}\right)_{\varepsilon_z} \quad \text{when } \sigma_\theta = \sigma_r = 0 \tag{6}$$

and

$$\mathrm{P} = \left(\frac{\varepsilon_z}{\varepsilon_r}\right)_{\varepsilon_\theta} \quad \text{when } \sigma_z = \sigma_r = 0 \tag{7}$$

In Eq. (5), σ_g, σ_r, σ_θ, and σ_z are generalized, radial, hoop, and axial stresses, respectively. For a thin-walled tubing where σ_r can be safely assumed to be zero, Eq. (5) reduces to the following expression.

$$\sigma_g = \left(\frac{\mathrm{R}\alpha^2 + (\alpha - 1)^2\mathrm{RP} + \mathrm{P}}{\mathrm{P}(\mathrm{R} + 1)}\right)^{1/2} \sigma_z \tag{8}$$

For evaluating R and P, the following expression are used.

$$\beta = \frac{\dot{\varepsilon}_\theta}{\dot{\varepsilon}_z} = \frac{\mathrm{R}}{\mathrm{P}}, \quad \text{for equi-biaxial loading } (\alpha = 1) \tag{9}$$

$$\rho = \frac{\dot{\varepsilon}_\theta}{\dot{\varepsilon}_r} = \frac{\mathrm{RP}(1 - \alpha) - R\alpha}{\mathrm{R}\alpha + \mathrm{P}} = \mathrm{R} \text{ for uniaxial loading } (\alpha = 0) \tag{10}$$

$$\mathrm{P} = \frac{\alpha}{1 - \alpha} \quad \text{for } \rho = 0 \tag{11}$$

To calculate R and P, ρ $(\dot{\varepsilon}_\theta/\dot{\varepsilon}_r)$ versus α curve was plotted as shown in Fig. 7. To evaluate β, steady-state $\dot{\varepsilon}_\theta$ and $\dot{\varepsilon}_z$ were obtained from biaxial creep test corresponding to $\alpha = 1$. To get the best estimate of initial value of R, the following expression was used [14].

$$\mathrm{R} = \cot^2 \bar{\phi} \tag{12}$$

where angle $\bar{\phi}$ represents basal pole peak angle in the transverse (ND-TD) plane. From Fig. 2c, the maximum intensity of the basal pole texture was found to be at $\sim 35°$, and R was found to be equal to 1.42. Using Eq. (9) P was obtained. Subsequently, different values of R (and P) were used in Eq. (10) to get a best fit of experimental data points as shown in Fig. 7 using dashed line and the best fit corresponded to R and P were found to be 1.25 and 1.08, respectively.

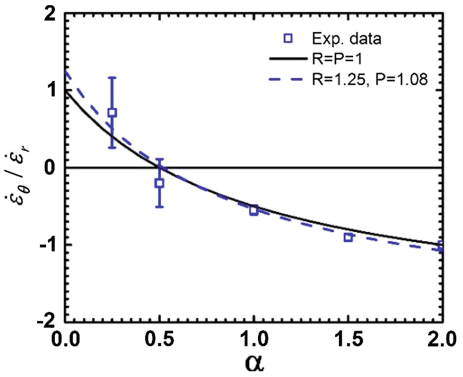

Fig. 7 Strain-rate ratio versus stress ratio for biaxial creep of HANA-4 alloy

Equation (11) can also be used to estimate P, and at ρ (= $\dot{\varepsilon}_\theta/\dot{\varepsilon}_r$) = 0, α was found to be 0.51. It resulted in P to be equal to 1.04 which is very close to what was obtained iteratively changing the values of R and P [using Eq. (9)]. In addition to the experimental data and fitting curve, another curve corresponding to isotropic deformation condition (R = P = 1) has been included in Fig. 7.

Creep Loci of the HANA-4 Alloy

A material's resistance against creep deformation is depicted using creep loci for multiaxial loading condition. Such creep loci are plotted at constant dissipation rate ($\dot{W}$) defined for biaxial loading of a tube by [17, 19]:

$$\dot{W} = \sigma_\theta \dot{\varepsilon}_\theta + \sigma_z \dot{\varepsilon}_z. \tag{13}$$

Using Eq. (13), a plot between $\dot{W}$ and σ_z was created for different loading ratios α (Fig. 8a). A log-linear relationship between these two parameters is evident from Fig. 8a and all the curves corresponding to different loading ratio are parallel to each other. A creep locus was created for $\dot{W}$ = 10 J m^{-3} s^{-1} and the plot is included in Fig. 8b. Open symbols in Fig. 8b represent experimental data points. Solid line was drawn using Eq. (7) by substituting R = 1.25 and P = 1.08. For dashed line, R = P = 1 was used in Eq. (7). A close proximity between solid line (anisotropic condition) and dashed line (isotropic condition) indicates a near isotropic creep deformation behavior of HANA-4 alloy.

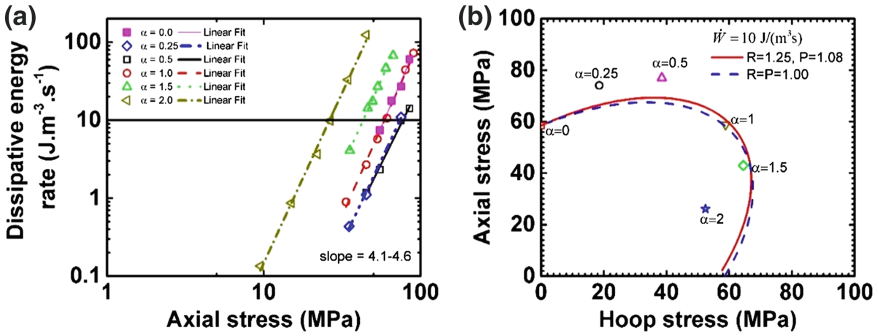

Fig. 8 **a** Log-log plot of dissipation energy rate versus axial stress as a function of stress ratio and **b** creep loci for 10 J/(m^3 s) dissipation energy rate

Comparison of Current Experimental Creep Results with Other Alloys

Figure 9 shows comparison of creep loci of HANA-4 with Zircaloy-4 and Zirlo [25]. As mentioned earlier, the creep loci of recrystallized HANA-4 is in close correspondence with the creep locus for isotropic condition (R = P = 1). Comparison of the creep loci of HANA-4 with that of Zircaloy-4 and Zirlo in Fig. 9 informs a highly anisotropic nature of creep for these two alloys (in recrystallized condition) compared to HANA-4.

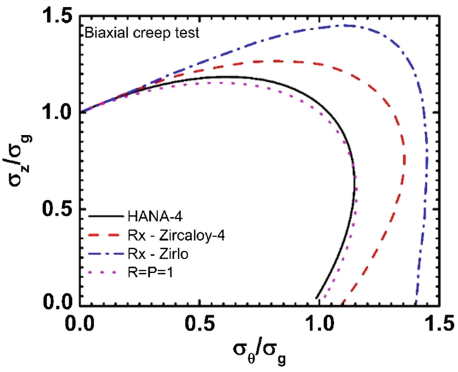

Fig. 9 Comparison of creep loci of HANA-4 with recrystallized Zircaloy-4 [19] and Zirlo [25]

Biaxial Anisotropic Creep Modeling Using Plasticity-CODF Model

Pole figures and inverse pole figures are commonly used to discuss texture in polycrystalline materials and effect of texture on anisotropic mechanical properties can be described qualitatively. Orientation distribution function is employed for a quantitative description of texture which allows one to determine volume fraction of crystallite orientations with respect to a given sample frame of reference. The probability a crystallite has Euler angles θ, ψ, φ with respect to the specimen axes is expressed as a series of generalized spherical harmonics,

$$\omega(\theta,\psi,\varphi) = \sum_{l=0}^{\infty} \sum_{m=-l}^{l} \sum_{n=-l}^{l} W_{lmn} Z_{lmn}(\cos\theta) \mathrm{e}^{-\mathrm{i}m\psi} \mathrm{e}^{-\mathrm{i}n\varphi} \tag{14}$$

where W_{lmn} and Z_{lmn} are termed as series coefficients and augmented Jacobi polynomials, respectively. The function $\omega(\theta, \psi, \varphi)$ is known as the crystallite orientation distribution function (CODF). The CODF can be used for predicting the mechanical properties of polycrystalline materials. The average property of a polycrystalline aggregate $\langle \rho(\theta,\psi,\varphi) \rangle$ is given as

$$\langle \rho(\theta,\psi,\varphi) \rangle = \int_0^{2\pi} \int_0^{2\pi} \int_{-1}^{1} \rho(\theta,\psi,\varphi)\omega(\theta,\psi,\varphi) d(\cos\theta) d\psi d\varphi \tag{15}$$

For strain-rate determination in the crystallite during creep $\rho(\theta, \psi, \varphi)$ will be replaced with $\dot{\varepsilon}_{ij}$ in Eq. (15). For predicting creep anisotropy in polycrystalline materials two important considerations are deformation by slip and evaluation of CODF. As outlined above, texture measurement using techniques such as XRD and EBSD allows one to evaluate CODF. Different plasticity theories taking dislocation slip for plastic deformation into account can be used along with CODF to account for anisotropic creep deformation of a polycrystalline aggregate. Power law creep is used to describe dependence of creep rate on stress and accordingly

$$\dot{\gamma}^k = A \left(\frac{\tau^k}{\tau_0^k} \right)^n \tag{16}$$

where A, τ_0, and n are the reference strain-rate, reference shear stress on the kth slip system, and stress exponent, respectively. The total strain-rate in the crystal is expressed as the sum of contributions from each of the active slip systems.

$$\dot{\varepsilon}_{ij}^c = \sum_k \mu_{ij}^k \dot{\gamma}^k \tag{17}$$

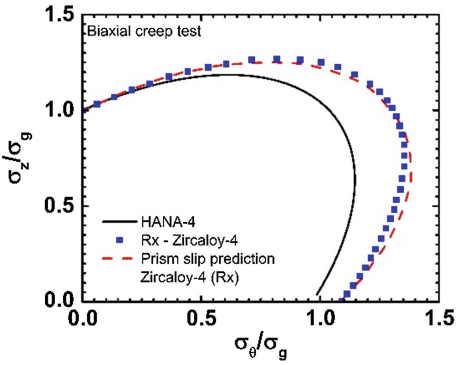

Fig. 10 Creep loci of HANA-4 and Zircaloy-4 with model prediction for Zircaloy-4 assuming prismatic slip [19]

where μ_{ij} is the geometric tensor connecting slip coordinates with crystal coordinates.

Using Eqs. (15)–(17) along with $\tau^k = \sigma_{ij}^c \mu_{ij}^k$, a creep locus was predicted for Rx-Zircaloy-4, as shown in Fig. 10 [19].

Summary and Conclusions

The HANA-4 alloy developed by Korea Atomic Energy Research Institute was subjected to biaxial creep testing in annealed (at 537 °C for 4 h) condition. All the tests were carried at a constant temperature of 500 °C and different hoop to axial stress ratios (0–2). From the dissipative energy rate versus axial stress plot, the power-law stress exponent was found to be in the range 3.1–3.5 (the slope of the curve in Fig. 8a represents n + 1). By using a modified von Mises yield criterion for anisotropic material, anisotropy parameters R and P were found to be equal to 1.25 and 1.08, respectively. These values of R and P were used to fit the experimental data points of the creep locus of the HANA-4 alloy. The comparison of the HANA-4 creep locus with that of Zircaloy and Zirlo cladding materials in similar microstructural state revealed less anisotropy of creep deformation in the HANA-4 alloy. Further comparison with creep locus corresponding to R = P = 1 confirmed planar isotropic creep deformation condition for the currently investigated alloy.

Acknowledgement This research was supported by NSF grant #DMR0968825.

References

1. Climate Action & The United Nations Environment Programme (2015), http://www.cop21paris.org/. Last accessed on 13 June 2016

2. Nuclear Energy Institute, Nuclear Energy Representation at the UN Climate Conference in Paris (2016), http://www.nei.org/News-Media/Media-Room/Media-Briefings/Nuclear-Energy-Representation-at-the-UN-Climate-Co. Last accessed on 13 June 2016
3. S.J. Zinkle, G.S. Was, Materials challenges in nuclear energy. Acta. Mater. **61**, 735–758 (2013)
4. J.A.L. Robertson, Zirconium—an international nuclear material. J. Nucl. Mater. **100**, 108–118 (1981)
5. D.O. Northwood, The development and applications of zirconium alloys. Mater. Des. **6**, 58–70 (1985)
6. C.R.F. Azevedo, Selection of fuel cladding material for nuclear fission reactors. Eng. Fail. Anal. **18**, 1943–1962 (2011)
7. K.L. Murty, I. Charit, *An Introduction to Nuclear Materials: Fundamentals and Applications* (Wiley VCH, 2013)
8. P. Frankel, J. Wei, E. Francis, A. Forsey, N. Ni, S. Lozano-Perez, A. Ambard, M. Blat-Yrieix, R. Comstock, L. Hallstadius, Effect of Sn on corrosion mechanisms in advanced Zr-cladding for pressurised water reactors, in *Zirconium in the Nuclear Industry*, vol. 17, ASTM International, 2015
9. Y.H. Jeong, S. Park, M. Lee, B. Choi, J. Baek, J. Park, J. Kim, H. Kim, Out-of-pile and in-pile perfomance of advanded zirconium alloys (HANA) for high burn-up fuel. J. Nucl. Sci. Technol. **43**, 977–983 (2006)
10. I. Charit, K.L. Murty, Creep behavior of niobium-modified zirconium alloys. J. Nucl. Mater. **374**, 354–363 (2008)
11. M.H. Yoo, Slip, twinning, and fracture in hexagonal close-packed metals. Metall. Trans. A **12**, 409–418 (1981)
12. R.G. Ballinger, G.E. Lucas, R.M. Pelloux, The effect of plastic strain on the evolution of crystallographic texture in Zircaloy-2. J. Nucl. Mater. **126**, 53–69 (1984)
13. E. Tenckhoff, *Deformation Mechanisms, Texture, and Anisotropy in Zirconium and Zircaloy* (ASTM International, 1988)
14. K.L. Murty, I. Charit, Texture development and anisotropic deformation of Zircaloys. Prog. Nucl. Energy **48**, 325–359 (2006)
15. B. Clay, The biaxial creep measurement of thin walled tubes. J. Mater. Sci. **9**, 1275–1278 (1974)
16. A. Donaldson, R. Horwood, T. Healey, *Biaxial Creep Deformation of Zircaloy-4 in the High Alpha Phase Temperature Range* (1983), pp. 103–118
17. K.L. Murty, B.L. Adams, Biaxial creep of textured zircaloy I: experimental and phenomenological descriptions. Mater. Sci. Eng. **70**, 169–180 (1985)
18. K. Murty, B. Tanikella, J. Earthman, Effect of grain shape and texture on equi-biaxial creep of stress relieved and recrystallized zircaloy-4. Acta. Metall. Mater. **42**, 3653–3661 (1994)
19. K. Murty, Zircaloy life prediction and new generation zircaloys for LWRs. Trans Indian Inst Met **50**, 533–562 (1997)
20. V. Venkatesan, S.T. Mahmood, K.L. Murty, Biaxial creep testing of textured Ti-3Al-2.5 V tubing. Metall. Trans. A **21**, 3001–3010 (1990)
21. C. Grosjean, D. Poquillon, J. Salabura, J. Cloué, Experimental creep behaviour determination of cladding tube materials under multi-axial loadings. Mater. Sci. Eng. A **510**, 332–336 (2009)
22. M. Mathew, S. Ravi, V. Vijayanand, S. Latha, A. Dasgupta, K. Laha, Biaxial creep deformation behavior of Fe–14Cr–15Ni–Ti modified austenitic stainless steel fuel cladding tube for sodium cooled fast reactor. Nucl. Eng. Des. **275**, 17–22 (2014)
23. B. Kombaiah, K.L. Murty, Coble, Orowan strengthening, and dislocation climb mechanisms in a Nb-modified Zircaloy cladding. Metall. Mater. Trans. A **46**, 4646–4660 (2015)
24. R. Hill, *A Theory of the Yielding and Plastic Flow of Anisotropic Metals*, vol. 193 (1948), pp. 281–297
25. I. Charit, J. Yan, B. Marple, K. Murty, Effects of alloying and thermal treatment on creep anisotropy of zircaloys: application to in-reactor performance. Mater. Sci. Technol. AIST **1**, 4 (2005)

Springer

http://www.springer.com/978-3-319-51096-5

Mechanical and Creep Behavior of Advanced Materials
A SMD Symposium Honoring Professor K. Linga Murty
Charit, I.; Zhu, Y.T.; Maloy, S.A.; Liaw, P.K. (Eds.)
2017, XIX, 293 p. 184 illus., Hardcover
ISBN: 978-3-319-51096-5